Research Article

Received: 4 June 2021 Accepted article published: 1 August 2021 Published online in Wiley Online Library: 21 August 2021

(wileyonlinelibrary.com) DOI 10.1002/pi.6282

Immiscible PHB/PBS and PHB/PBSA blends: morphology, phase composition and modelling of elastic modulus

Maria Cristina Righetti,[a*] Patrizia Cinelli,[b*] Laura Aliotta,[b] Elisa Bianchi,[b] Fabio Tricoli,[a] Maurizia Seggiani[b] and Andrea Lazzeri[a,b]

Abstract

This paper reports the thermal, morphological and mechanical properties of environmentally friendly poly(3-hydroxybutyrate) (PHB)/poly(butylene succinate) (PBS) and PHB/poly[(butylene succinate)-*co*-(butylene adipate)] (PBSA) blends, prepared by melt mixing. The blends are known to be immiscible, as also confirmed by the thermodynamic analysis here presented. A detailed quantification of the crystalline and amorphous fractions was performed, in order to interpret the mechanical properties of the blends. As expected, the ductility increased with increasing PBS or PBSA amount, but in parallel the decrease in the elastic modulus appeared limited. Surprisingly, the elastic modulus was found properly described by the rule of mixtures in the whole composition range, thus attesting mechanical compatibility between the two blend components. This unusual behavior has been explained as due to co-continuous morphology, present in a wide composition range, but also at the same time as the result of shrinkage occurring during sequential crystallization of the two components, which can lead to physical adhesion between matrix and dispersed phase. For the first time, the elastic moduli of the crystalline and mobile amorphous fractions of PBS and PBSA and of the mobile amorphous fraction of PHB at ambient temperature have been estimated through a mechanical modelling approach.

Supporting information may be found in the online version of this article.

Keywords: immiscible blends; crystallization; co-continuous morphology; physical adhesion; elastic modulus

INTRODUCTION

Poly(3-hydroxybutyrate) (PHB) is a compostable, biodegradable and biocompatible polymer belonging to the polyhydroxyalkanoate family, produced by several bacteria as intracellular carbon reserve.[1,2] These favorable characteristics of PHB are unfortunately counterbalanced by poor mechanical properties and intrinsic brittleness. For these reasons practical applications of PHB are strongly limited.[3] It is known that PHB undergoes progressive embrittlement upon storage, due to additional crystallization occurring at ambient temperature (T_{room}).[4] The gradual increase in crystallinity, as a consequence of the growth of secondary crystals in geometrically restricted areas, was found to increase also the constrained amorphous regions located in proximity of the crystals, thus causing further progressive PHB embrittlement.[5] These constrained amorphous regions constitute the so-called called rigid amorphous fraction (RAF), whereas the amorphous areas far from the crystal surfaces form the mobile amorphous fraction (MAF).[6]

To reduce the brittleness of PHB, copolymerization with various hydroxyalkanoate units has been applied. Poly[(3-hydroxybutyrate)-*co*-(3-hydroxyvalerate)]s (PHBV), the most common random copolymers of PHB, exhibit lower fragility and higher elongation at break with respect to PHB.[7] Otherwise, PHB can be blended with biobased or biodegradable polymers. Polymer blending is an economic and useful way to modify the properties of PHB. By changing the composition of the mixture, materials with suitable properties for various applications can be obtained. To improve ductility, PHB has been mixed with polymers characterized by high toughness and low glass transition temperature (T_g) values, as for example poly(ethylene oxide),[8] poly(ε-caprolactone),[9] poly(butylene succinate) (PBS),[10–13] poly[(butylene succinate)-*co*-(butylene adipate)] (PBSA),[14] poly[(butylene adipate)-*co*-(butylene terephthalate)][15] and poly(propylene carbonate).[16]

* *Correspondence to: MC Righetti, CNR-IPCF, National Research Council, Institute for Chemical and Physical Processes, Via Moruzzi 1, Pisa, 56124, Italy. E-mail: cristina.righetti@pi.ipcf.cnr.it (Righetti); or P Cinelli, Department of Civil and Industrial Engineering, University of Pisa, Largo Lazzarino 1, Pisa, 56122, Italy. E-mail: patrizia.cinelli@unipi.it (Cinelli)*

a *CNR-IPCF, National Research Council, Institute for Chemical and Physical Processes, Via Moruzzi 1, Pisa, 56124, Italy*

b *Department of Civil and Industrial Engineering, University of Pisa, Largo Lazzarino 1, Pisa, 56122, Italy*

In particular, PBS is a very interesting aliphatic polyester, because it can be biobased as PHB, besides being biodegradable, as well as the copolymers PBSA. PBS and PBSA exhibit good melt processability, chemical resistance and mechanical properties as common polyolefins.[17] PBSA copolymers are characterized by isodimorphism, i.e. co-crystallization of the co-monomers in the crystal lattices of the two homopolymers PBS and poly(butylene adipate). The co-monomer incorporation depends on the composition, and is generally modest.[18]

Investigations of the properties of blends of PHB or PHBV and PBS or PBSA, prepared both by melt mixing and solvent casting, demonstrated that a biphasic system is generally obtained over the whole composition range.[10–13,19–21] The morphology of the melt-blended PHB/PBS mixtures was found to change from dispersed phase to a continuous distribution, with a co-continuous morphology for PHB/PBS 50/50 and 30/70.[12]

In the study presented here, the mechanical properties of melt-blended PHB/PBS and PHB/PBSA mixtures were investigated in the whole composition range, and interpreted as a function of the phase composition and morphology. Compatibilizers were not added, to make the blends more economical and sustainable. In the literature, mechanical properties of the PHB/PBS and PHBV/PBS blends can be found referred to partial composition intervals.[11,21] The only study that reports mechanical properties data determined in the entire composition range refers to blends of PBS and PHBV (5 mol% of hydroxyvalerate units),[20] with a higher hydroxyvalerate content with respect to the PHB grade used in the present study.

However, the present study takes a step forward, with the interpretation of the elastic modulus trend as a function of the morphology and solidification process of the two blend components, and with a modelling of the elastic modulus on the basis of the crystalline and amorphous fractions of the two blend components. A connection between the blend elastic modulus and the elastic moduli of the different phases has been found. With this purpose, the elastic modulus of the PHB/PBS and PHB/PBSA blends has been theoretically described by expanding the two-phase Takayanagi model[22,23] to a multiple-phase system, in order to quantify the contribution of the different crystalline and amorphous fractions. The Takayanagi model is a combination of series and parallel elements to take into account the different deformations that separate phases undergo under stress. The two-phase Takayanagi model has been widely applied to the prediction of the elastic modulus of semicrystalline polymers,[24,25] blends,[26] copolymers[27] and composites.[28] By taking into account the amorphous and crystalline amounts of the two blend components, the elastic moduli of the crystalline and mobile amorphous regions of PBS and PBSA have been theoretically estimated, as well as the elastic modulus of the mobile amorphous fraction of PHB. To the best of our knowledge, this is the first time that these values have been assessed and reported.

MATERIALS AND METHODS

Materials

Commercial polyhydroxyalkanoate (grade PHI002™) in pellets was supplied by Naturplast® (Caen, France). The material is a PHBV copolymer with 1 mol% of hydroxyvalerate units.[29] The melt flow index test, performed by means of a CEAST M20 melt flow tester, according to the standard ISO 1133:2005, led to a MFR of 1.9 ± 0.8 g (10 min)$^{-1}$ (190 °C, 0.325 kg) and a viscosity of 810 ± 200 Pa s. The melting temperature of PHI002™ was identical to that of pure PHB (T_m = 172 °C); thus, due the very low amount of hydroxyvalerate units, the polymer is here labelled PHB.

Commercial biobased PBS and PBSA (BioPBS™, grade FZ91PM and FD92PM) in pellets were provided by PTT MCC Biochem (Bangkok, Thailand). The butylene adipate amount in PBSA is 20 mol%.[30] The melt flow index test led to a MFR of 3.6 ± 0.5 and 0.65 ± 0.01 g (10 min)$^{-1}$ (190 °C, 0.325 kg) and a viscosity of 480 ± 50 and 728 ± 100 Pa s for PBS and PBSA, respectively.

Blend preparation

The composition (in wt%) of the PHB/PBS and PHB/PBSA blends investigated was: 85/15, 70/30, 50/50, 30/70, 15/85. Unmixed PHB and PBS or PBSA were labelled 100/0 and 0/100, respectively.

Before processing, PHB, PBS and PBSA were dried for 24 h in a Piovan DP 604-615 dryer (Piovan SPA, Verona, Italy) at 60 °C to eliminate traces of humidity. The PHB/PBS and PHB/PBSA blends were prepared using a Haake MiniLab II (Thermo Fisher Scientific, Waltham, MA, USA), a co-rotating conical twin-screw extruder. The pellets of the two components were roughly mixed in the appropriate weight percentage, and then poured into the mini extruder. Successively the molten materials were transferred through a preheated cylinder to the mini injection molder (Haake MiniJet II, Thermo Fisher Scientific), which allows the preparation of bar specimens, to be used for thermal and mechanical characterization. The dimensions of the dog-bone bars for tensile tests were: width in the larger section: 10 mm; width in the narrow section: 4.8 mm; thickness: 1.35 mm; length: 90 mm. The extruder operating conditions adopted for the blends are reported in Table 1. After preparation, all the samples were stored in a desiccator. As the mechanical properties of PHB change upon storage at T_{room}, due to additional crystallization and RAF increase,[4,5] the thermal and mechanical characterizations were performed simultaneously 2 days after the preparation of the blends.

Blend characterization

DSC measurements were performed with a DSC 8500 calorimeter (PerkinElmer, Waltham, MA, USA) equipped with an IntraCooler III as refrigerating system. The instrument was calibrated in temperature with high-purity standards (indium, naphthalene, cyclohexane) according to the procedure for standard DSC.[31] Enthalpy calibration was performed with indium. Dry nitrogen was used

Table 1. Operating conditions for the extrusion and injection molding processes

PHB/PBS PHB/PBSA	Extrusion temperature (°C)	Screw speed (rpm)	Cycle time (s)	Injection temperature (°C)	Injection pressure (bar)	Molding time (s)	Mold temperature (°C)
100/0 and all the blends	175	100	90	175	150	60	60
0/100	155	100	90	155	150	60	60

as purge gas at a rate of 20 mL min^{-1}. To gain precise heat capacity data from the heat flow rate measurements, each scan was accompanied by an empty pan run (blank run), with the mass of the blank and sample aluminium pans matching within 0.02 mg. To reduce as much as possible the thermal lag, the sample mass was lower than 10 mg. All the as-prepared blends were analyzed from −85 to 200 °C at a heating rate of 10 K min^{-1}, after quick cooling from T_{room}. In addition, the PHB/PBS and PHB/PBSA blends were analyzed upon cooling from the melt at 50 K min^{-1}, to mimic approximately the processing conditions, and subsequently upon heating at 10 K min^{-1}.

Tensile tests were performed at T_{room}, at a crosshead speed of 10 mm min^{-1}, by means of an Instron 5500R universal testing machine (Canton MA, USA), equipped with a 10 kN load cell and interfaced with a computer running Testworks 4.0 software (MTS Systems Corporation, Eden Prairie, MN, USA). At least five specimens were tested for each sample according to ASTM D 638, and the average values were reported.

The morphology of the blend surfaces was obtained using SEM with an FEG Quanta 450 (Thermo Fisher, Waltham, MA, USA). Micrographs of samples fractured with liquid nitrogen and etched with gold, by means of an Edward S150B sputter coater, were collected. Backscattered electrons generated the images with resolution provided by beam deceleration with a landing energy of 2 kV.

RESULTS AND DISCUSSION

Thermal characterization

Figure 1 collects the apparent specific heat capacity ($c_{p,app}$) curves of the as-prepared PHB/PBS and PHB/PBSA blends, together with the thermodynamic solid and liquid specific heat capacities (c_p^s and c_p^l for PHB, PBS and PBSA; $c_{p,blend}^s$ and $c_{p,blend}^l$ for the blends). For PHB, the expressions $c_p^s = 1.21 + 0.0035T$ and $c_p^l = 1.72 + 0.0022T$ were used,[32] whereas for PBS and PBSA, $c_p^s = 1.21 + 0.0030T$ and $c_p^l = 1.79 + 0.0016T$ were applied, with the solid and liquid specific heat capacities expressed in J g^{-1} K^{-1} and T in °C.[33]

For all the mixtures, the $c_{p,app}$ data in the solid and liquid states were found to be in perfect agreement with thermodynamic solid and liquid specific heat capacities ($c_{p,blend}^s$ and $c_{p,blend}^l$ respectively), calculated as the weighted sum of c_p^s and c_p^l of the two components, according to the relationships $c_{p,blend}^s(T) = \Sigma\ W_i\ c_{p,i}^s(T)$ and $c_{p,blend}^l(T) = \Sigma\ W_i\ c_{p,i}^l(T)$, where W_i is the weight fraction of the ith component. The absence of specific interactions between PHB and PBS or PBSA is proven by the null contribution of excess specific heat capacity to the thermodynamic $c_{p,blend}^s$ and $c_{p,blend}^l$.[33]

The enlargements of the curves show that T_g of the semicrystalline PBS is centered at about −32 °C, whereas that of the copolymer PBSA appears located at lower temperatures (−46 °C), due to the higher mobility of the butylene adipate units, in agreement with literature data.[18,34] Because of the high crystallinity of the as-prepared PHB, the $c_{p,app}$ increment at T_g is barely recognizable around 5 °C. In the PBS- and PBSA-rich blends, T_g appears unchanged with respect to plain PBS and PBSA, as well as in the PHB-rich blends, where a single T_g is present at temperatures slightly above 0 °C, as in plain PHB. Also, for the intermediate compositions, unmodified glass transitions can be observed, although more barely due to the reduced percentage of the two components. As monotonic change in T_g from the glass transition of PHB to the glass transition of PBS or PBSA is not observed with a change in the blend composition, the immiscibility of the PHB/PBS and PHB/PBSA blends is confirmed. At temperatures higher than T_g, around 60 °C, the $c_{p,app}$ curve of PHB exhibits a large endotherm, which was previously connected to the devitrification of the RAF together with an enthalpy recovery process connected to RAF physical aging.[35]

Also, the melting endotherms of the blends appear unchanged with respect to plain PHB and PBS or PBSA, although the area progressively decreases as a consequence of the changed composition. The main melting peak of PHB is centered at 172 °C. Multiple endotherms characterize the fusion of PBS and PBSA, due to the occurrence of melting and recrystallization processes upon heating.[33,36,37] Both PBS and PBSA exhibit a small

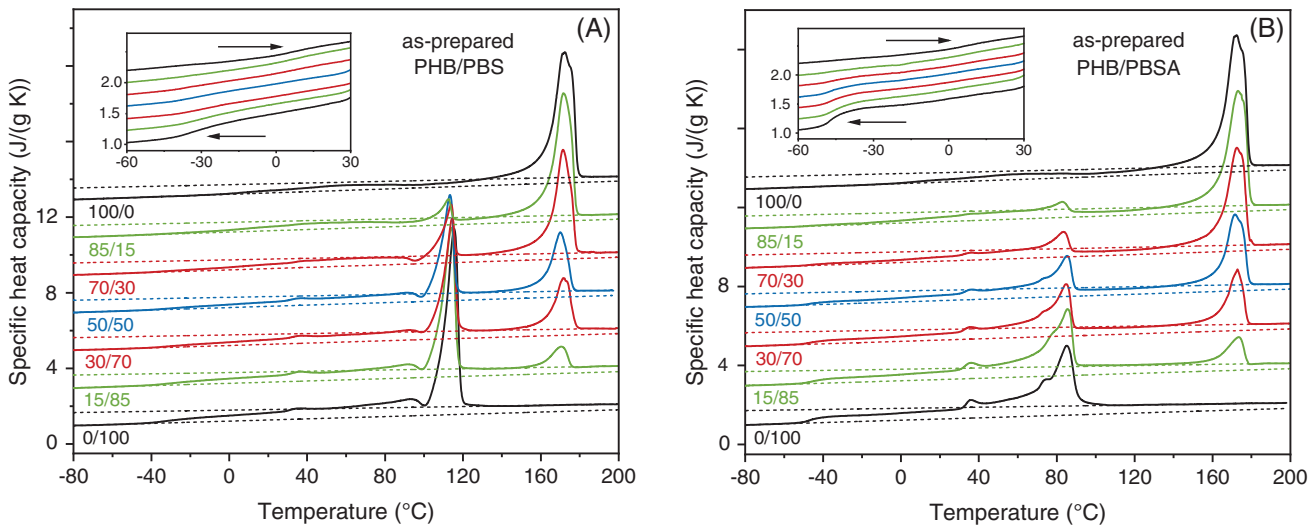

Figure 1. Apparent specific heat capacity ($c_{p,app}$) of the as-prepared (A) PHB/PBS and (B) PHB/PBSA blends (solid lines) as a function of temperature, at a heating rate of 10 K min^{-1}. The dotted lines are the thermodynamic solid and liquid specific heat capacities of PHB, PBS, PBSA and the PHB/PBS and PHB/PBSA blends (see text). The ordinate values refer only to the bottom curve (PBS and PBSA curves). All the other curves are shifted vertically for the sake of clarity. In the inset, an enlargement of the $c_{p,app}$ curves in the T_g region is shown. The arrows mark the glass transition of the blend components.

endotherm around 40 °C, probably connected to the fusion of defective crystal grown at T_{room} during the two-day storage subsequent to preparation, whereas the main melting peaks are located at 115 and 86 °C, respectively.

The crystalline and the amorphous weight fractions of all the as-prepared samples were determined from the $c_{p,app}$ curves depicted in Fig. 1. The total MAF of the blends (w_{MA}) was determined at 20 °C through Eqn (1):

$$w_{MA}(T) = \frac{c_{p,app}(T) - c_p^s(T)}{c_p^l(T) - c_p^s(T)} \quad (1)$$

because 20 °C, which is above T_g of all the respective components, is the temperature at which the mechanical analysis was performed. From the separate enthalpies of melting of PHB ($\Delta h_{m,PHBV}$), PBS ($\Delta h_{m,PBS}$) and PBSA ($\Delta h_{m,PBSA}$) the contributions of the single components to the crystalline weight fraction of the blend were determined ($w_{C,PHB}$, $w_{C,PBS}$, $w_{C,PBSA}$, respectively), as $w_{C,i} = \Delta h_{m,i}/\Delta h_{m,i}^{\circ}$, where Δh_m° is the melting enthalpy of 100% crystalline polymers ($\Delta h_{m,PHB}^{\circ} = 144$ J g^{-1}[32] and $\Delta h_{m,PBS}^{\circ} = \Delta h_{m,PBSA}^{\circ} = 200$ J g^{-1}[38,39]). The units of $\Delta h_{m,i}$ are (J g_{blend}^{-1}), whereas those of $\Delta h_{m,i}^{\circ}$ are (J g_i^{-1}); thus the calculated $w_{C,i}$ values are the contributions of the single components to the crystallinity of the mixture. The total crystalline weight fraction (w_C) was obtained as the sum of the distinct crystalline fractions.

Finally, the RAF (w_{RA}) at 20 °C was determined by difference: $w_{RA} = 1 - w_C - w_{MA}$. The experimental $\Delta h_{m,i}$ data, as well as the calculated $w_{C,i}$, w_{MA} and w_{RA} values are listed in Tables S1 and S2 in the supporting information. The data in the tables highlight that at 20 °C, w_{RA} is approximately 10% in PHB and zero in PBS and PBSA.

Figure 2 shows the evolution of the separate and total crystalline fractions, and the total MAF and RAF for the PHB/PBS and PHB/PBSA blends as a function of the composition. All the variations are linear, due to the thermodynamic immiscibility of the PHB/PBS and PHB/PBSA systems. The crystallinity of the copolymer PBSA is lower with respect to the homopolymer PBS, in agreement with literature data.[18,34] The RAF increases with $w_{C,PHB}$, thus confirming that it is located exclusively at the PHB amorphous/crystal interphase. Tables S1 and S2 in the supporting information show that the crystallinities of the separate PHB, PBS and PBSA, calculated as $w_{C,i}^{\circ} = w_{C,i}/W_i$, are approximately constant, quite high (about 60% for PHB, 40% for PBS and 30% for PBSA) and independent of the blend composition, which further confirm that crystallization of each component occurs approximately independently in separated areas.

After melting, the PHB/PBS and PHB/PBSA blends were also analyzed upon cooling at 50 K min^{-1} (Fig. 3). Two separate crystallization peaks in different crystallization ranges can be observed, which proves that crystallization of the two components of the blends occurs sequentially. The crystallization of PHB, with a peak at 102 °C, shifts to slightly lower temperatures with increasing PBS and PBSA amount, likely due to the presence of melted domains of PBS or PBSA in proximity to the crystallization growth front, which can interfere with the crystal growth.[40,41] Conversely, crystallization of PBS and PBSA turned out to be favored by the presence of PHB, because of being shifted to slightly higher temperatures with respect to the plain polymers. Evidently, PHB crystals act as nucleation points for PBS and PBSA crystallization. The assisted heterogeneous nucleation attests that the interfaces wet well the crystallizable PBS or PBSA, which means that a certain compatibility exists between PHB and PBS or PBSA. The supporting information collects the $c_{p,app}$ curves of the PHB/PBS and PHB/PBSA blends at 10 K min^{-1} after cooling at 50 K min^{-1} (Fig. S1), from which the evolution of the crystalline, mobile amorphous and rigid amorphous fractions was derived, confirming the linear trends observed for the as-prepared samples (Fig. S2). The calculated amorphous and crystalline fractions appear almost identical to the corresponding values of the as-prepared samples.

Morphological characterization

The morphology of cryo-fractured surfaces of PHB, PBS and PBSA and the respective blends was examined using SEM, in order to investigate the dispersion of the two polymers in the blends. Figure 4 illustrates the topology of the blends at ×20 000 magnification, whereas the surfaces of pure PHB, PBS and PBSA and all the blends at ×10 000 magnification are reported in the supporting information (Fig. S3). Pure PHB shows a smooth surface, which indicates a brittle behavior. Conversely, the fracture surfaces of

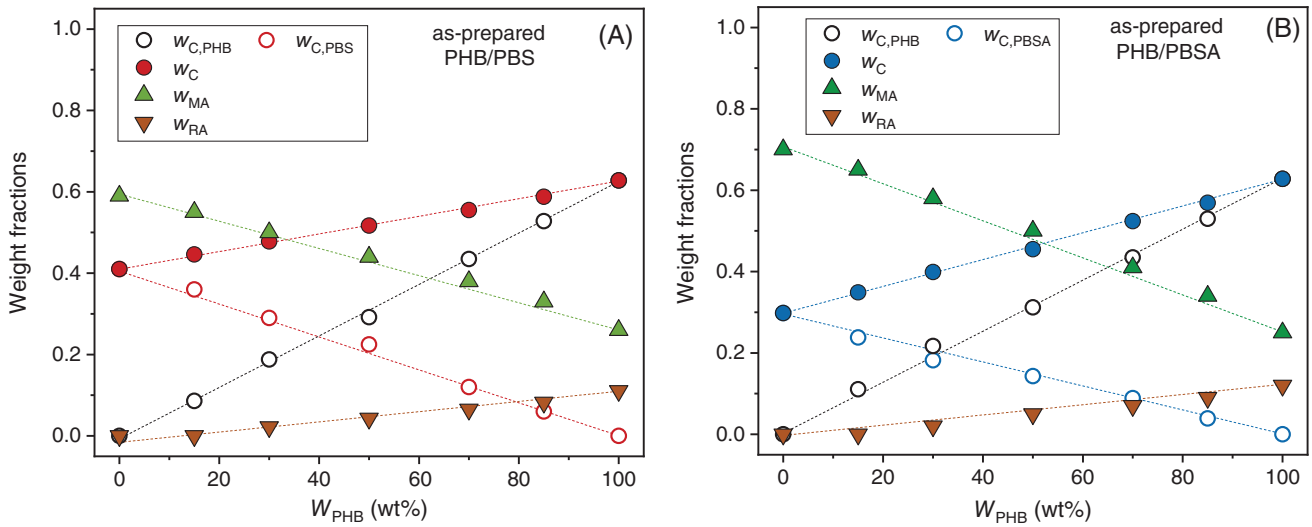

Figure 2. Crystalline weight fraction of PHB ($w_{C,PHB}$), crystalline weight fraction of (A) PBS and (B) PBSA ($w_{C,PBS}$ and $w_{C,PBSA}$), total crystalline weight fraction (w_C), total MAF (w_{MA}) at 20 °C, total RAF (w_{RA}) at 20 °C for the as-prepared (A) PHB/PBS and (B) PHB/PBSA blends as a function of blend composition (estimated errors: ±0.02 for $w_{C,PHB}$, $w_{C,PBS}$ and $w_{C,PBSA}$; ±0.02 for w_{MA}; ±0.04 for w_C; ±0.06 for w_{RA}). The lines are guides to the eye.

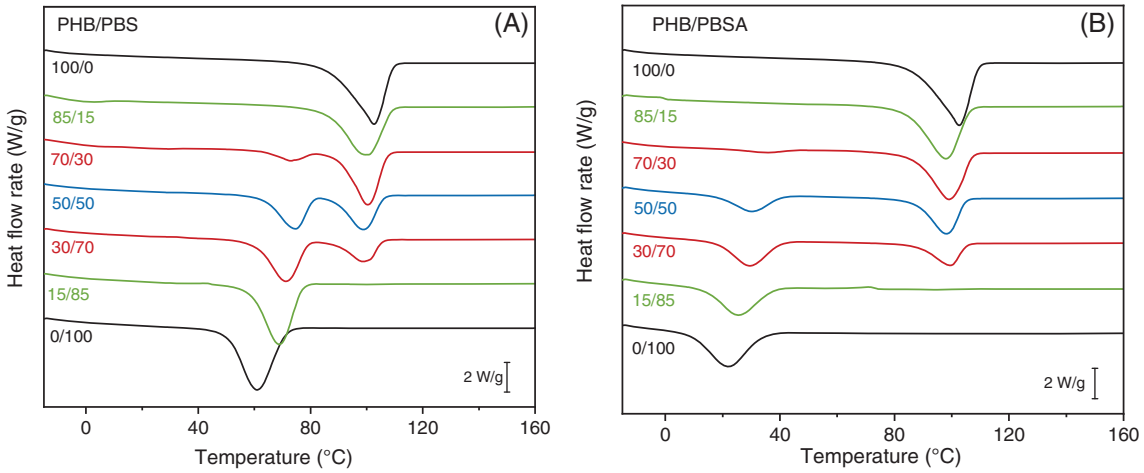

Figure 3. Heat flow rate curves of (A) PHB/PBS and (B) PHB/PBSA blends upon cooling at 50 K min^{-1} as a function of temperature.

PBS and PBSA appear rougher, due to their more ductile performance.

The surfaces of the PHB/PBS and PHB/PBSA 15/85 and 85/15 blends are similar, and show the typical matrix–droplets morphology. The dispersion is homogeneous, and the average droplet size is about 0.5 μm. It is worth noting that the small white particles, visible in the PHB-rich blends, have been attributed in previous studies to inorganic fillers present in commercial PHB.[42] The droplet size increases with an increase in the second phase amount, as visible for the PHB/PBSA 70/30 blend. Conversely, the morphology of the parallel PHB/PBS 70/30 blend appears different: the separation of the two components is less evident, and the appearance is more similar to that of the PHB/PBS and PHB/PBSA 50/50 blends, which clearly exhibit a co-continuous morphology, as well as both the 30/70 mixtures. Thus, the composition range in which the co-continuous morphology develops in the PHB/PBS blends is broader with respect to the PHB/PBSA blends.

In the co-continuous phase morphology, the distribution of the two components is interconnected and continuous. This morphology originates from the coalescence of the droplets with increasing separate polymer amount, and depends on the rheological properties and mixing conditions.[40,41] Generally, a co-continuous morphology is found around the phase inversion composition, which is defined as[43]

$$\varphi_{1,PI} = \frac{1}{1+\theta} \quad (2)$$

with $\theta = \eta_2/\eta_1$, where η_i are the viscosities of the blend components. Using the viscosity values estimated by MFR measurements (η_{PHB} = 810 Pa s, η_{PBS} = 480 Pa s and η_{PBSA} = 728 Pa s), $\varphi_{PHB,PI}$ = 0.63 for the PHB/PBS blends and $\varphi_{PHB,PI}$ = 0.52 for the PHB/PBSA blends were determined. This φ_{PI} assessment, although approximate, is in excellent agreement with the morphological observations.

For the PHB/PBS and PHB/PBSA 50/50 co-continuous blends, the voids between the two separate phases are really negligible (about 0.05 μm) and the phase size is about 0.5–1 μm; thus good mechanical properties are expected. The time stability of the co-continuous morphology at T_{room} is guaranteed for the PHB/PBS and PHB/PBSA blends by the high degree of crystallinity that develops at higher temperatures.

Tensile properties

The stress (σ) *versus* strain (ε) curves of the as-prepared PHB/PBS and PHB/PBSA blends at T_{room} are shown in Fig. 5, whereas the values of the elastic modulus (E), tensile strength at break and elongation at break are listed in Table S3 of the supporting information. The tensile tests revealed that the fracture behavior changes from brittle, for PHB, to progressively more ductile for the blends. The PHB/PBS and PHB/PBSA 85/15 blends did not exhibit necking formation, which conversely was observed for the 70/30 and 50/50 blends. Well evident necking with stable growth was displayed by the PBS- and PBSA-rich blends. Due to the higher mobility that characterizes PBSA with respect to PBS, strain hardening, likely due to chain alignment, was observed in association with neck growth for the PBSA-rich blends. Strain hardening is however observed also for pure PBS. The final fracture for the PBS- and PBSA-rich blends occurred at a significantly increased elongation, compared with that for the neat PHB.

Figure 6 shows the elastic modulus of the PHB/PBS and PHB/PBSA blends as a function of the volumetric composition V_i (the volume fraction of the ith component), determined as reported in the supporting information and listed in Tables S4 and S5. Together with the experimental E data, Fig. 6 displays also the E values calculated using the parallel and series mechanical coupling models, which suppose a parallel and a series arrangement of the two blend components, and represent the upper and lower bounds of the tensile modulus predictions.[44] For the parallel model, $E = V_1E_1 + V_2E_2$, whereas for the series model $1/E = V_1/E_1 + V_2/E_2$, where E_i are the elastic moduli of blend components and V_i are the corresponding volume fractions. In addition, Fig. 6 reports the elastic modulus calculated according to the Davies model ($E^{1/5} = V_1{E_1}^{1/5} + V_2{E_2}^{1/5}$),[45] often utilized to predict the modulus of co-continuous blends. It can be observed that the Davies model underestimates the modulus of the co-continuous PHB/PBS and PHB/PBSA blends, as well as the quite complex equations recently derived by Veenstra *et al*. to differentiate droplet–matrix and co-continuous morphologies, according to tri-dimensional arrangements of parallel and series elements (here not reported).[46]

Many immiscible blends exhibit a sigmoidal E trend as a function of composition, with the modulus of the blends richest in the softer component approaching the lower bound, and the

Polymer International published by John Wiley & Sons Ltd on behalf of Society of Industrial Chemistry.

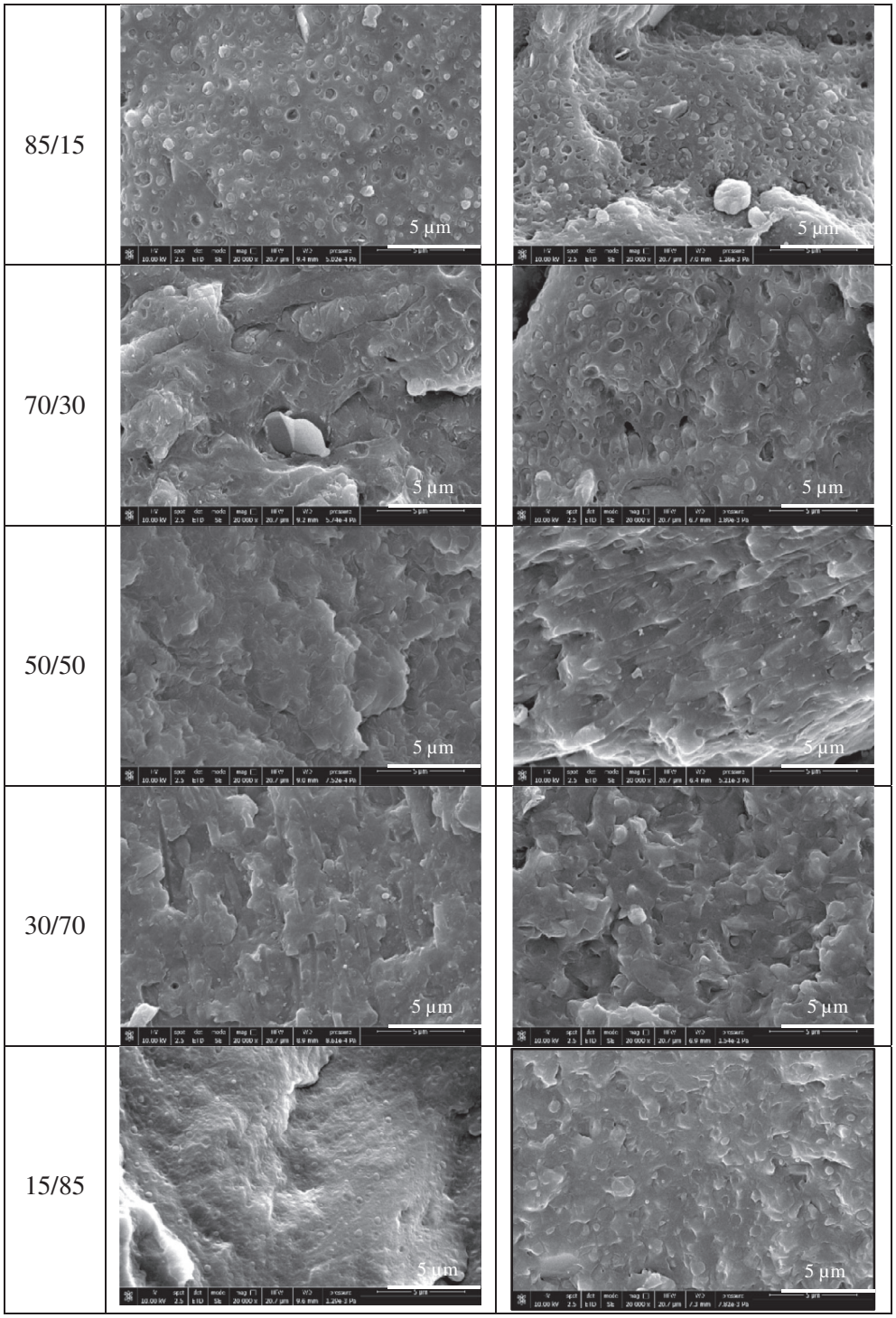

Figure 4. SEM images at ×20 000 of the PHB/PBS (left column) and PHB/PBSA (right column) blends.

modulus of the blends richest in the stiffer component tending to the upper bound.[47,48] The transition from one behavior to the other occurs in the region of co-continuity and phase inversion. Generally, the elastic modulus of co-continuous blends is significantly higher than that of blends with dispersed morphology,[46] and often it approaches the value predicted by the rule of mixtures, because this morphology is able to favor good stress transfer due to the strong connection of the two components.[43]

The most important result deducible from Fig. 6 is that for the PHB/PBS and PHB/PBSA blends, *E* is described by the rule of mixtures not only in the co-continuous range, but in the whole composition range. The good agreement between the experimental *E* values and the prediction of the rule of mixtures in the whole composition range suggests that, despite the thermodynamic immiscibility of the PHB/PBS and PHB/PBS blends, a sort of physical adhesion exists between the matrix and the dispersed

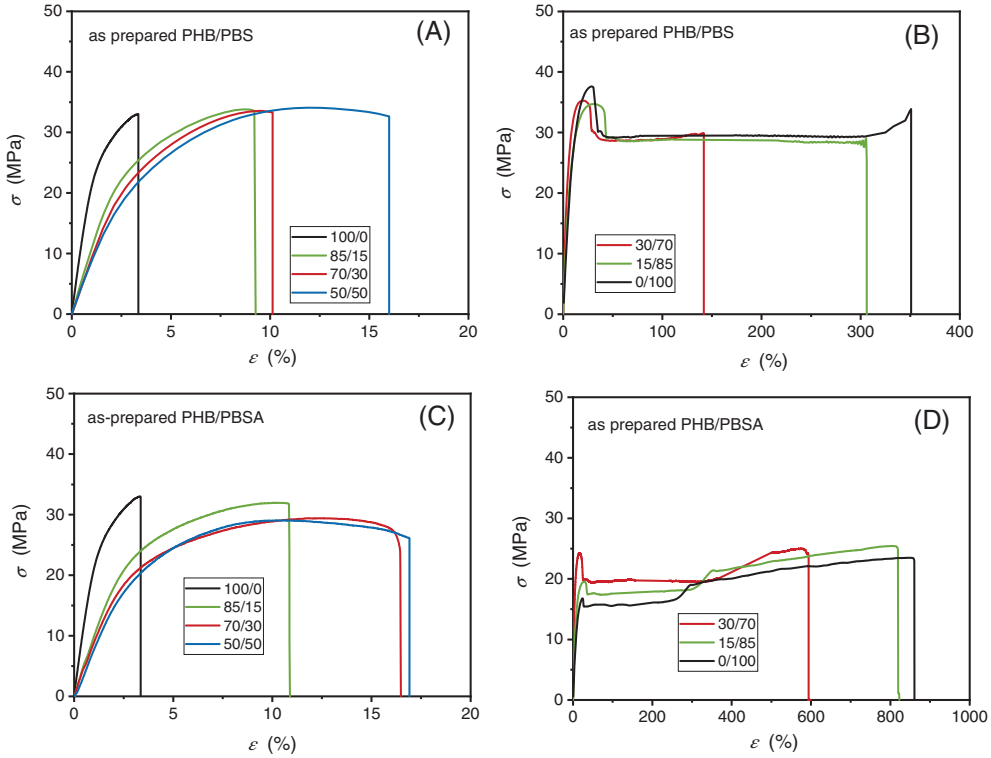

Figure 5. Stress–strain (σ *versus* ε) curves of the as-prepared (A, B) PHB/PBS and (C, D) PHB/PBSA blends measured at T_{room}.

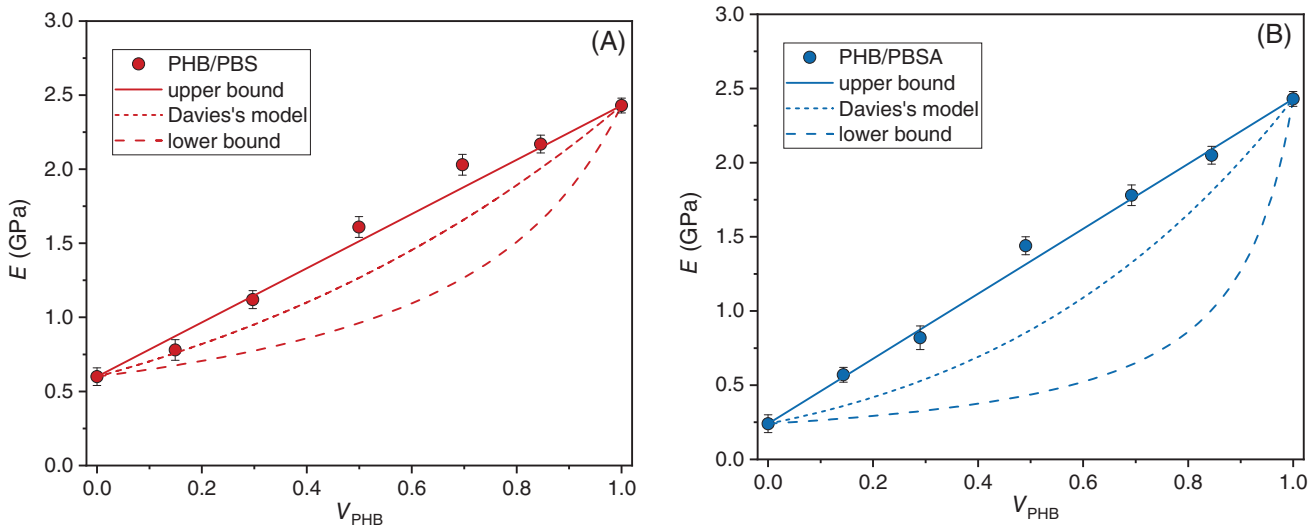

Figure 6. Elastic modulus (E) of the as-prepared (A) PHB/PBS and (B) PHB/PBSA blends as a function of volumetric composition. The solid, dashed and short dashed lines are the elastic modulus predictions according to the parallel model (upper bound), the series model (lower bound) and the Davies model, respectively.

phases.[49] This physical junction could be ascribed to the shrinkage that the two components undergo during crystallization. PHB crystallizes with a high degree of crystallinity at higher temperature, before PBS and PBSA. In the PBS- and PBSA-rich blends, the PBS and PBSA contraction upon crystallization takes place in the presence of the dispersed and already crystallized PHB regions, which can favor interfacial contact between the two components. The same mechanism in the PHB-rich blends can lead to restricted PBS and PBSA domains, as a consequence of the PHB crystallization. This interpretation can account for the high elastic modulus exhibited by the PHB/PBS and PHB/PBSA blends not only in the co-continuous regions, but also in the presence of phase-separated morphology. Thus, despite the immiscibility of the blend components, the rule of mixtures can be the result of concomitant co-continuous morphology and physical adhesion between the two blend components. These effects together can explain the mechanical compatibility exhibited by the PHB/PBS and PHB/PBSA blends.

Polymer International published by John Wiley & Sons Ltd on behalf of Society of Industrial Chemistry.

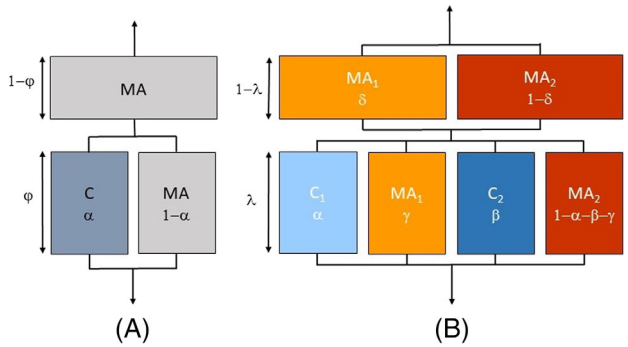

Figure 7. Schematic representation of (A) the two-phase Takayanagi model and (B) the multiple-phase Takayanagi model used to describe the PHB/PBS and PHB/PBSA blends.

Modelling of elastic modulus

In the original Takayanagi model, the amorphous and the crystalline phases of a semicrystalline polymer are arranged in a combination of series and parallel positions, to represent different conditions of good and poor stress transfer. For semicrystalline polymers the series–parallel model (i.e. the amorphous phase in series with a parallel combination of the amorphous and crystalline phases, as shown in Fig. 7(A)) was found to better interpret the strain distribution under stress.[50] In the model, the texture parameters α and φ are connected to the phase composition, being $\alpha\varphi = V_C$, where V_C is the volumetric fraction of the crystalline phase.

To describe the elastic behavior of the immiscible PHB/PBS and PHB/PBSA blends, by taking into account the strong interconnections between PHB and PBS or PBSA as a consequence of the co-continuous morphology present in a wide composition range and the physical junction resulting from crystallization shrinkage, the MAFs of the two components (MA_1 and MA_2) were organized in series with all the crystalline (C_1 and C_2) and amorphous fractions put in parallel (Fig. 7(B)). The contribution of the RAF, present in low percentage, is neglected. The equation that describes the elastic modulus of the blends according to the configuration of Fig. 7(B) is

$$\frac{1}{E}=\frac{1-\lambda}{\delta E_{MA,1}+(1-\delta)E_{MA,2}}+\frac{\lambda}{\alpha E_{C,1}+\beta E_{C,2}+\gamma E_{MA,1}+(1-\alpha-\beta-\gamma)E_{MA,2}} \quad (3)$$

The texture parameters λ, δ, α and β are linked to the phase composition, being $\alpha\lambda = V_{C,1}$, $\beta\lambda = V_{C,2}$ and $V_1 = \alpha\lambda + \gamma\lambda + \delta(1-\lambda)$, where $V_{C,i}$ are the volumetric fractions of the crystalline phases (calculated as reported in the supporting information) and V_1 the volumetric fraction of component 1. After the substitutions $\alpha = V_{C,1}/\lambda$, $\beta = V_{C,2}/\lambda$ and $\gamma = [V_1 - V_{C,1} - \delta(1-\lambda)]/\lambda$, Eqn (3) becomes

$$\frac{1}{E}=\frac{1-\lambda}{\delta E_{MA,1}+(1-\delta)E_{MA,2}}+\frac{\lambda^2}{V_{C,1}E_{C,1}+V_{C,2}E_{C,2}+[V_1-V_{C,1}-\delta(1-\lambda)]E_{MA,1}+[\lambda-V_1-V_{C,2}+\delta(1-\lambda)]E_{MA,2}} \quad (4)$$

Table 2. Volumetric fractions of crystalline PHB and PBS phases ($V_{C,PHB}$ and $V_{C,PBS}$), texture parameters λ and δ, elastic modulus of crystalline PBS phase ($E_{C,2} = E_{C,PBS}$) and elastic modulus of MAFs of PHB ($E_{MA,1} = E_{MA,PHB}$) and PBS ($E_{MA,2} = E_{MA,PBS}$) predicted by Eqn (4)

PHB/PBS	$V_{C,PHB}$	$V_{C,PBS}$	λ	δ	$E_{C,2} = E_{C,PBS}$ (GPa)	$E_{MA,1} = E_{MA,PHB}$ (GPa)	$E_{MA,2} = E_{MA,PBS}$ (GPa)
100/0	0.61	0.00	0.97	1.00	—	0.28	—
85/15	0.51	0.06	0.97	0.94	2.90	0.25	0.22
70/30	0.42	0.11	0.96	0.92	2.98	0.29	0.18
50/50	0.29	0.21	0.95	0.86	2.95	0.26	0.20
30/70	0.19	0.27	0.88	0.81	2.97	0.28	0.17
15/85	0.09	0.34	0.76	0.72	2.98	0.32	0.15
0/100	0.00	0.39	0.67	0.00	2.99	—	0.26
					2.96 ± 0.03	*0.28 ± 0.02*	*0.20 ± 0.04*

The values in italics are the average $E_{C,PBS}$, $E_{MA,PHB}$ and $E_{MA,PBS}$ values, with respective standard deviations.

Table 3. Volumetric fractions of crystalline PHB and PBSA phases ($V_{C,PHB}$ and $V_{C,PBSA}$), texture parameters γ and δ, elastic modulus of crystalline PBSA phase ($E_{C,2} = E_{C,PBSA}$) and elastic modulus of MAFs of PHB ($E_{MA,1} = E_{MA,PHBV}$) and PBSA ($E_{MA,2} = E_{MA,PBSA}$) predicted by Eqn (4)

PHB/PBSA	$V_{C,PHB}$	$V_{C,PBS}$	λ	δ	$E_{C,2} = E_{C,PBSA}$ (GPa)	$E_{MA,1} = E_{MA,PHB}$ (GPa)	$E_{MA,2} = E_{MA,PBSA}$ (GPa)
100/0	0.61	0.00	0.97	1.00	—	0.28	—
85/15	0.51	0.04	0.96	0.94	2.50	0.26	0.22
70/30	0.42	0.08	0.95	0.91	2.55	0.28	0.15
50/50	0.30	0.13	0.94	0.87	2.42	0.25	0.18
30/70	0.21	0.17	0.83	0.77	2.42	0.24	0.17
15/85	0.11	0.22	0.73	0.67	2.34	0.26	0.13
0/100	0.00	0.28	0.37	0.00	2.40	—	0.16
					2.44 ± 0.07	*0.26 ± 0.02*	*0.17 ± 0.03*

The values in italics are the average $E_{C,PBSA}$, $E_{MA,PHB}$ and $E_{MA,PBSA}$ values, with respective standard deviations.

where the unknown quantities are $E_{C,1}$, $E_{C,2}$, $E_{MA,1}$, $E_{MA,2}$, δ and λ. The theoretical value of the elastic modulus of the crystalline PHB phase, available in the literature, was maintained fixed ($E_{C,1} = E_{C,PHB} = 5$ GPa),[51] and to estimate the parameters $E_{C,2}$, $E_{MA,1}$, $E_{MA,2}$, δ and λ, an iterative process was carried out by minimizing the error between the experimental and the theoretical elastic moduli predicted by Eqn (4) (by means of Excel® Data Solver Function). The initial values for the fitting procedure were determined by assuming, as a first approximation, that $E_{MA,1} = E_{MA,2}$ because the T_g values of PHB, PBS and PBSA are all below T_{room}. The results of the minimization procedure are reported in Tables 2 and 3 for the PHB/PBS and PHB/PBSA blends, respectively.

All the data listed in Tables 2 and 3 appear consistent. The texture parameter λ changes accordingly with the overall crystallinity, attesting that it is correctly connected with the blocks containing the crystalline phases. Also, parameter δ changes in agreement with the composition, as it decreases with the amount of PHB. Interesting outcomes are the elastic moduli of PBS and PBSA, which, to the best of our knowledge, have never been measured or theoretically estimated. The elastic modulus of crystalline PBS phase ($E_{C,PBS} = 3.0$ GPa) turns out to be in good agreement with the approximate value determined from a group contribution method described by van Krevelen and te Nijenhuis,[52] which predicts a tensile modulus of 3.4 GPa. As expected, the elastic modulus of the crystalline PBSA phase ($E_{C,PBSA} = 2.4$ GPa) comes out lower than that of PBS, because the inclusion of butylene adipate units in the PBS lattice induces higher cell dimensions,[18] and therefore a greater possibility for elastic chain rearrangements under stress.

Polymer chain straightening and alignment through rotations around bonds is the main mechanism of elastic deformation of the MAF; thus the order $E_{MA,PHB}$ (= 0.27 GPa) > $E_{MA,PBS}$ (= 0.20 GPa) > $E_{MA,PBSA}$ (= 0.17 GPa) reflects the facility of chain conformation rearrangements, and therefore the T_g sequence. The value $E_{MA,PHB} = 0.27$ GPa is correctly slightly higher than the experimental values reported in the literature for some copolymers of PHB containing co-units with higher mobility ($E_{MA} = 0.22$ GPa for a copolymer with $T_g = -8$ °C and composition hydroxybutyrate (94 mol%) + medium-chain-length hydroxyalkanotes (6 mol%)[53]; and $E_{MA} = 0.13$ GPa for a copolymer with $T_g = -7$ °C and composition hydroxybutyrate (73 mol%) + hydroxyvalerate (13 mol%) + hydroxyheptanoate (14 mol%)[54]). To the best of our knowledge, this is the first estimation of the elastic moduli of the MAF of PHB and the crystalline phases and MAFs of PBS and PBSA at T_{room}.

CONCLUSIONS

Environmentally friendly mixtures PHB/PBS and PHB/PBSA, without the addition of compatibilizers, have been prepared by melt mixing, in order to reduce the PHB brittleness. The specific heat capacities of the mixtures in the solid and liquid states were found to be in perfect agreement with the weighted sum of the c_p values of the two components, attesting to the absence of specific interactions between PHB and PBS or PBSA. The crystallinity of PHB, PBS and PBSA was quite high (about 60% for PHB, 40% for PBS and 30% for PBSA), and approximately constant, independent of blend composition, which confirmed that crystallization of each component takes place in separated domains. Co-continuous morphology was found in a wide central composition range for both PHB/PBS and PHB/PBSA blends, whereas the typical matrix–droplets morphology was present in the PHB- and PBS- or PBSA-rich blends. The spaces between the two separate phases appeared negligible.

As expected, the ductility of the blends increased with PBS or PBSA. In parallel, the elastic modulus decreased, but the reduction appeared limited. Unexpectedly, in the whole composition range the elastic modulus of the PHB/PBS and PHB/PBSA blends obeyed the rule of mixtures, which represents the upper limit for the elastic modulus. Equations usually utilized to predict the elastic modulus of immiscible blends, also in the presence of co-continuous morphology, were found to underestimate the E values. An interpretation based on shrinkage connected to the crystallization in sequence of the two components has been provided. The successive solidification of the two crystalline phases can lead to good physical contact and mechanical junction between the two components, with the result that the PHB/PBS and PHB/PBSA blends appear mechanically compatible. In conclusion, the addition of PBS or PBSA to PHB not only provides materials with higher flexibility with respect to pure PHB, but also guarantees good stiffness to the blends.

By means of a modelling approach, for the first time the elastic moduli of the MAF of PHB and the crystalline phases and MAFs of PBS and PBSA at T_{room} have been estimated. To the best of our knowledge, this is the first time that these E_C and E_{MAF} values have been reported.

ACKNOWLEDGEMENT

The authors thank Dr. Randa Ishak for her valuable support in carrying out the SEM analysis.

SUPPORTING INFORMATION

Supporting information may be found in the online version of this article.

REFERENCES

1 Sudesh K, Abe H and Doi Y, *Prog Polym Sci* **25**:1503–1555 (2000).
2 Bugnicourt E, Cinelli P, Lazzeri A and Alvarez V, *Express Polym Lett* **8**: 791–808 (2014).
3 Chuan Yeo JC, Muiruri JK, Thitsartarn W, Li Z and He C, *Mater Sci Eng C* **92**:1092–1116 (2018).
4 de Koning GJM, Scheeren AHC, Lemstra PJ, Peeters M and Reynaers H, *Polymer* **35**:4598–4605 (1994).
5 Di Lorenzo ML and Righetti MC, *Eur Polym J* **49**:510–517 (2013).
6 Wunderlich B, *Prog Polym Sci* **28**:383–450 (2003).
7 Laycock B, Halley P, Pratt S, Werker A and Lant P, *Prog Polym Sci* **39**: 397–442 (2014).
8 Avella M, Martuscelli E and Greco P, *Polymer* **32**:1647–1653 (1991).
9 Gassner F and Owen AJ, *Polymer* **35**:2233–2236 (1994).
10 Qiu Z, Ikehara T and Nishi T, *Polymer* **44**:2503–2508 (2003).
11 Ma P, Hristova-Bogaerds DG, Lemstra PJ, Zhang Y and Wang S, *Macromol Mater Eng* **297**:402–410 (2012).
12 Ma P, Hristova-Bogaerds DG, Zhang Y and Lemstra PJ, *Polym Bull* **71**: 907–923 (2014).
13 Ma P, Cai X, Wang W, Duan F, Shi D and Lemstra PJ, *J Appl Polym Sci* **131**:41020 (2014).
14 Salomez M, George M, Fabre P, Touchaleaume F, Cesar G, Lajarrige A *et al.*, *Polym Degrad Stab* **167**:102–113 (2019).
15 Costa ARM, Reul LTA, Sousa FM, Ito EN, Carvalho LH and Canedo EL, *Polym Test* **69**:266–275 (2018).
16 Zhang S, Sun X, Ren Z, Li H and Yan S, *Phys Chem Chem Phys* **17**:32225–32231 (2015).
17 Xu J and Guo B-H, *Biotechnol J* **5**:1149–1163 (2010).
18 Perez-Camargo RA, Fernandez-d'Arlas B, Cavallo D, Debuissy T, Pollet E, Averous L *et al.*, *Macromolecules* **50**:597–608 (2017).

19 Qiu Z, Ikehara T and Nishi T, *Polymer* **44**:7519–7527 (2003).
20 Phua YJ, Pegoretti A, Medeiros Araujo T and Mohd Ishak ZA, *J Appl Polym Sci* **132**:42815 (2015).
21 Jost V and Miesbauer O, *J Appl Polym Sci* **135**:46153 (2018).
22 Takayanagi M, Uemura S and Minami S, *J Polym Sci Part C Polym Symp* **5**:113–122 (1964).
23 Takayanagi M, Imada K and Kajiyama T, *J Polym Sci Part C Polym Symp* **15**:263–281 (1967).
24 Montes de Oca H and Ward IM, *Polymer* **47**:7070–7077 (2006).
25 Aliotta L, Cinelli P, Coltelli MB, Righetti MC, Gazzano M and Lazzeri A, *Eur Polym J* **93**:822–832 (2017).
26 Woo EM, Su CC, Kuo J-F and Seferis JC, *Macromolecules* **27**:5291–5296 (1994).
27 Stanford JL, Young RJ and Day RJ, *Polymer* **32**:1713–1725 (1991).
28 Li F, Gao Y and Jiang W, *Polymer* **170**:101–106 (2019).
29 Jost V, *Express Polym Lett* **12**:429–435 (2018).
30 Malz F, Arndt J-H, Balko J, Barton B, Büsse T, Imhof D *et al.*, *J Chromatogr A* **1638**:461819 (2021).
31 Sarge SM, Hemminger W, Gmelin E, Höhne GWH, Cammenga HK and Eysel W, *J Thermal Anal* **49**:1125–1134 (1997).
32 Righetti MC, Tombari E and Di Lorenzo ML, *J Phys Chem B* **117**:12303–12311 (2013).
33 Signori F, Pelagaggi M, Bronco S and Righetti MC, *Thermochim Acta* **543**:74–81 (2012).
34 Debuissy T, Pollet E and Averous L, *Eur Polym J* **87**:84–98 (2017).
35 Di Lorenzo ML, Gazzano M and Righetti MC, *Macromolecules* **45**:5684–5691 (2012).
36 Yoo ES and Im SS, *J Polym Sci Polym Phys* **37**:1357–1366 (1999).
37 Yasuniwa M, Tsubakihara S, Satou T and Iura K, *J Polym Sci Polym Phys* **43**:2039–2047 (2005).
38 Miyata T and Masuku T, *Polymer* **39**:1399–1404 (1998).
39 Papageorgiou GZ and Bikiaris DN, *Polymer* **46**:12081–12092 (2005).
40 Groeninckx G, Harrats C, Vanneste M and Everaert V, Crystallization, micro- and nano-structure, and melting behavior of polymer blends, in *Polymer Blends Handbook*, ed. by Utracki LA and Wilkie CA. Springer, Dordrecht, pp. 291–446 (2003).
41 Tien N-D and Prud'homme RE, Crystallization behavior of semicrystalline immiscible polymer blends, in *Crystallization in Multiphase Polymer Systems*, ed. by Thomas S, Arif PM, Gowd EB and Kalarikkal N. Elsevier, Amsterdam, pp. 181–212 (2018).
42 Corre Y-M, Bruzaud S, Audic J-L and Grohens Y, *Polym Test* **31**:226–235 (2012).
43 Pötschke P and Paul DR, *Polym Rev* **43**:87–141 (2003).
44 Ahmed S and Jones FR, *J Mater Sci* **25**:4933–4942 (1990).
45 Davies WEA, *J Phys D* **4**:1325–1339 (1971).
46 Veenstra H, Verkooijen PCJ, van Lent BJJ, van Dam J, de Boer AP and Nijhof APHJ, *Polymer* **41**:1817–1826 (2000).
47 Stoclet G, Seguela R and Lefebvre J-M, *Polymer* **52**:1417–1425 (2011).
48 Simoes CL, Viana JC and Cunha AM, *J Appl Polym Sci* **112**:345–352 (2009).
49 Leclair A and Favis BD, *Polymer* **37**:4723–4728 (1996).
50 Aliotta L, Gazzano M, Lazzeri A and Righetti MC, *ACS Omega* **5**:20890–20902 (2020).
51 Wang H and Tashiro K, *Macromolecules* **49**:581–594 (2016).
52 van Krevelen DW and te Nijenhuis K, *Properties of Polymers*, 2nd edn. Elsevier, Amsterdam, pp. 383–522 (2009).
53 Matsusaki H, Abe H and Doi Y, *Biomacromolecules* **1**:17–22 (2000).
54 Li SY, Dong CL, Wang SY, Ye HM and Chen G-Q, *Appl Microbiol Biotechnol* **90**:659–669 (2011).